THE JOURNAL OF BIOLOGICAL CHEMISTRY VOL. 288, NO. 14, pp. 9801–9814, April 5, 2013

Cross-talk between Tetraspanin CD9 and Transmembrane Adaptor Protein Non-T Cell Activation Linker (NTAL) in Mast Cell Activation and Chemotaxis*

Received for publication, December 27, 2012, and in revised form, February 21, 2013 Published, JBC Papers in Press, February 26, 2013, DOI 10.1074/jbc.M112.449231

Ivana Hálová, Lubica Dráberová, Monika Bambousková[1], Martin Machyna[2], Lucie Stegurová[1], Daniel Smrž[3], and Petr Dráber[4]

From the Department of Signal Transduction, Institute of Molecular Genetics, Academy of Sciences of the Czech Republic, CZ 14220 Prague, Czech Republic

Background: Chemotaxis is regulated by chemoattractants and poorly understood intrinsic regulators.
Results: Aggregation of tetraspanin CD9 leads to activation of mast cells and inhibition of their antigen-driven chemotaxis.
Conclusion: Chemotaxis toward antigen involves cross-talk between immunoreceptor, CD9, transmembrane adaptor proteins, and cytoskeleton-regulatory proteins.
Significance: Tetraspanin CD9 is defined as a novel regulator of mast cell chemotaxis.

Chemotaxis, a process leading to movement of cells toward increasing concentrations of chemoattractants, is essential, among others, for recruitment of mast cells within target tissues where they play an important role in innate and adaptive immunity. Chemotaxis is driven by chemoattractants, produced by various cell types, as well as by intrinsic cellular regulators, which are poorly understood. In this study we prepared a new mAb specific for the tetraspanin CD9. Binding of the antibody to bone marrow-derived mast cells triggered activation events that included cell degranulation, Ca^{2+} response, dephosphorylation of ezrin/radixin/moesin (ERM) family proteins, and potent tyrosine phosphorylation of the non-T cell activation linker (NTAL) but only weak phosphorylation of the linker for activation of T cells (LAT). Phosphorylation of the NTAL was observed with whole antibody but not with its $F(ab)_2$ or Fab fragments. This indicated involvement of the Fcγ receptors. As documented by electron microscopy of isolated plasma membrane sheets, CD9 colocalized with the high-affinity IgE receptor (FcεRI) and NTAL but not with LAT. Further tests showed that both anti-CD9 antibody and its $F(ab)_2$ fragment inhibited mast cell chemotaxis toward antigen. Experiments with bone marrow-derived mast cells deficient in NTAL and/or LAT revealed different roles of these two adaptors in antigen-driven chemotaxis. The combined data indicate that chemotaxis toward antigen is controlled in mast cells by a cross-talk among FcεRI, tetraspanin CD9, transmembrane adaptor proteins NTAL and LAT, and cytoskeleton-regulatory proteins of the ERM family.

Mast cells are derived from progenitors that are released from bone marrow into circulation, and subsequently migrate to peripheral tissues where they undergo differentiation and maturation (1). The process plays a vital role in innate and/or adaptive immune response and is controlled by a plethora of different chemoattractants, which require sophisticated mechanisms for their recognition and proper cellular responses (2–4). It is obvious that such mechanisms must involve efficient cross-talk between surface receptors, plasma membrane component organizers, such as tetraspanin, signal transducers, cytoskeletal effectors, and others. Signal transduction mediated by two important mast cell receptors, the high-affinity IgE receptor (FcεRI)[5] and the stem cell factor (SCF) receptor (KIT), is dependent on the presence of two transmembrane adaptor proteins (TRAPs), the linker for activated T cells (LAT) and the non-T cell activation linker (NTAL, also called LAB or LAT2) (5–8). Both adaptors are structurally similar and serve as plasma membrane docking sites for cytoplasmic signal transduction molecules. TRAPs are characterized by a short extracellular domain, a single transmembrane domain, and a cytoplasmic tail, which has no intrinsic enzymatic activity but possesses various tyrosine-containing motifs and domains. The properties of transmembrane domains and the presence of palmitoylation sites determine the solubility of LAT and NTAL in non-ionic detergents, distribution in the plasma membrane, and some other functional properties (9–11). Despite their

* This work was supported in part by the Projects 301/09/1826, P302/10/1759 and P302/12/G101, 204/09/H084 from Grant Agency of the Czech Republic, Action BM1007 from the European Cooperation in Science and Technology. Project LD12073 COST-CZ-MAST, Project TA01010436 of the Technology Agency of the Czech Republic, Project FR-TI3/067 of the Ministry of Industry and Trade of the Czech Republic, and Institutional Support Grant RVO 68378050.
[1] Supported in part by the Faculty of Science, Charles University, Prague, Czech Republic.
[2] Present address: Max Planck Institute of Molecular Cell Biology and Genetics, Dresden, Germany.
[3] Present address: Institute of Immunology, 2nd Medical School and University Hospital Motol, Charles University, V Úvalu 84, Prague, Czech Republic.
[4] To whom correspondence should be addressed: Laboratory of Signal Transduction, Institute of Molecular Genetics, Academy of Sciences of the Czech Republic, Vídeňská 1083, CZ-14220 Prague 4, Czech Republic. Tel.: 420-241062468; Fax: 420-241062214; E-mail: draberpe@img.cas.cz.

[5] The abbreviations used are: FcεRI, high-affinity IgE receptor; SCF, stem cell factor; TRAP, transmembrane adaptor protein; LAT, linker for activation of T cells; NTAL, non-T cell activation linker; KD, knockdown; BMMC, bone marrow-derived mast cell; Ag, antigen; ERM, ezrin/radixin/moesin; TNP, 2,4,6-trinitrophenol; 2KO, $Ntal^{-/-}/Lat^{-/-}$ double KO; BSS, buffered saline solution; BSSA, BSS supplemented with 0.1% BSA; $[Ca^{2+}]_i$, concentrations of intracellular Ca^{2+}; 2-PCCF, pair cross-correlation function; F-actin, filamentous actin.

structural similarity, NTAL and LAT were found in different microdomains in plasma membrane (5, 11). Studies with mast cells generated from NTAL or LAT KO mice (5, 6), human mast cells with NTAL knockdown (KD) (7), or rat basophilic leukemia cells with enhanced or reduced NTAL levels (12) showed that NTAL could act either as positive or negative regulator of FcεRI signaling, whereas LAT acts as positive regulator (4, 13). Although the role of these two adaptors in immunoreceptor signaling has been extensively studied, their function in mast cell migration is not fully understood. We have previously shown that NTAL serves as a negative regulator of bone marrow-derived mast cells (BMMCs) migration toward antigen (Ag) but has no apparent role in migration toward SCF (14). However, the role of LAT ablation either alone or together with NTAL on Ag-mediated chemotactic response is unknown.

Tetraspanins, similarly as TRAPs, have no enzymatic activity and regulate signaling events by cross-talk with other plasma membrane-associated protein molecules, including integrins (15–21), G-protein-coupled receptors (21–23), several immunoglobulin superfamily members (24, 25), and PKC (26). Although tetraspanins are involved in a variety of biological and pathological processes (27, 28), it is not clear whether tetraspanins interact with TRAPs and what are consequences of such interactions.

In this study we aggregated tetraspanin CD9 on the surface of mast cells and investigated signaling events elicited by such treatment. We also analyzed the effect of CD9 aggregation on cell activation events induced by Ag-mediated aggregation of the FcεRI, including degranulation, calcium response, phosphorylation of cytoskeleton-regulatory proteins of the ezrin/radixin/moesin (ERM) family, and chemotaxis. Using mast cells derived from NTAL- and/or LAT-deficient mice we studied a cross-talk of these adaptors with CD9 and its impact on mast cell chemotaxis. Finally, we investigated the role of CD9 in activation through the FcεRI and membrane topography of CD9 with respect to NTAL, LAT, and FcεRI. Our data indicate that chemotaxis toward Ag in mast cells is regulated by a cross-talk among CD9, FcεRI, TRAPs, and cytoskeleton-regulatory ERM family proteins.

EXPERIMENTAL PROCEDURES

Antibodies and Reagents—Anti-CD9 mAb (clone 2H9, IgG_1 type) was generated by immunizing a rat (Wistar strain) with BMMCs permeabilized with 0.1% saponin and washed. Hybridoma production and mAb selection was done as described previously (29) with the exception that rat spleen cells instead of mouse spleen cells were used. Specificity of the 2H9 antibody was verified by immunoprecipitation followed by mass spectrometry analysis as described (30) and by cross-immunoprecipitation using commercially available anti-CD9 antibody (KMC8.8, Santa Cruz Biotechnology, Inc.). Isotyping was performed with the IsoStrip Isotyping kit (Roche Diagnostics) following the manufacturer's protocol. $F(ab)_2$ and Fab fragments of the 2H9 antibody were generated using, respectively, $F(ab)_2$ and Fab Preparation Kits (Pierce) according to the manufacturer's protocol. Functionality of both types of the fragments was verified by FACS analysis and SDS-PAGE electrophoresis.

The following mAbs were used: 2,4,6-trinitrophenol (TNP)-specific IgE, clone IGEL b4 1 (31), anti-FcεRI β-subunit (JRK) (32), anti-NTAL (NAP-07) (33), anti-LAT (34), anti-Lyn (35), and anti-CD16/CD32 (2.4G2; directed against extracellular domains of mouse receptors FcγRIIB and FcγRIII; a gift from V. Horejsi). Polyclonal antibodies specific for LAT, NTAL, and IgE have been prepared in this laboratory after immunizing rabbits with the corresponding recombinant proteins or their fragments (36). Polyclonal antibodies specific for phospho-ERK (phospho-Y^{204}), phospho-Akt (phospho-S^{473}), phospho-c-Kit (phospho-$Y^{568/570}$), anti-integrin β1 (CD29), as well as HRP-conjugated goat anti-mouse IgG, and goat anti-rabbit IgG were obtained from Santa Cruz Biotechnology, Inc.; antibodies against phospho-p38 (Y^{182}/T^{180}; $pp38^{Y/T}$), phospho-Ezrin (T^{567})/Radixin (T^{564})/Moesin (T^{558}) ($pERM^{T}$), phospho-Syk (Y^{525}/Y^{526}; $pSyk^{Y}$), phospho-Akt (T^{308}; $pAkt^{T}$), and HRP-conjugated goat anti-rat IgG were obtained from Cell Signaling. Phospho-Tyr-specific mAb (PY-20) conjugated to HRP, anti-CD9 (KMC8), and anti-integrin β1 (HM β1–1) were purchased from BD Biosciences. Anti-mouse FcεRI-FITC conjugate and anti-mouse CD117 (KIT)-APC conjugate were obtained from eBioscience; anti-mouse integrin β1-FITC was from Millipore. Recombinant mouse IL-16 was obtained from Prospec. All other chemicals were obtained from Sigma.

Cells and Lentiviral Infection—BMMCs were derived from C57BL.6 mice of WT ($Ntal^{+/+}$ or $Lat^{+/+}$) or from $Ntal^{-/-}$, $Lat^{-/-}$ or $Ntal^{-/-}/Lat^{-/-}$ double KO (2KO) mice (5). In some experiments, Balb/c mice were also used as indicated in the text. All work with animals was conducted in accordance with institutional (33/2008) and national (2048/2004–1020) guidelines. Bone marrow cells were isolated and cultured as previously described (5). BMMCs deficient in Lyn ($Lyn^{-/-}$) and their WT controls ($Lyn^{+/+}$) were kindly provided by M. Hibbs (Ludwig Institute for Cancer Research, Melbourne, Australia) (37). HEK 293 T/17 packaging cells were purchased from American Type Culture Collection. The cells were grown as adherent monolayer culture in DMEM containing 10% FCS, 100 units/ml of penicillin, and 100 μg/ml of streptomycin. Cultures were passaged regularly every 4–5 days and kept at 37 °C in an atmosphere of 5% CO_2. The cells used for lentivirus production were at passage 4–15. Lentiviral infection was done as described previously (38). A set of murine CD9 shRNAs cloned into the pLKO.1 vector (TRCN0000066393, TRCN0000066394, TRCN0000066395, TRCN0000066396, and TRCN0000066397) were purchased from Open Biosystems. Stable selection was achieved by culturing the transfected cells for 2 weeks in the presence of puromycin (5 μg/ml). Cells were analyzed for CD9 expression by immunoblotting and FACS. Cells with the highest reduction of CD9 protein, obtained with TRCN0000066393 and TRCN0000066395, were selected for further experiments. Cells transfected with empty pLKO.1 vector were used as negative controls.

β-Glucuronidase Release, Ca^{2+} Response, Protein Phosphorylation, and Immunoprecipitation—BMMCs were sensitized in SCF- and IL-3-free culture medium supplemented with IGEL b4 1 mAb (1 μg/ml) for 16 h, unless stated otherwise. Then the cells were washed in buffered saline solution (BSS) supplemented with 0.1% BSA (BSSA), and activated with Ag (TNP-

BSA conjugate, 15–25 mol of TNP/mol of BSA; 100–500 ng/ml, depending on batch), SCF (20–100 ng/ml, depending on batch), or anti-CD9 (0.04–20 μg/ml) at concentrations and times giving maximum degranulation or protein phosphorylation, respectively. For inhibition experiments cells were pretreated with different concentrations of anti-CD9 mAb for 15 min. The extent of secretion was determined by determining the concentration of β-glucuronidase as described previously (39) except that the Infinite 200M (TECAN) plate reader instrument at excitation and emission wavelengths of 355 and 460 nm, respectively, was used. Cells used in calcium response assays were loaded with Fura-2AM as described previously (40) and changes in concentrations of intracellular Ca^{2+} ($[Ca^{2+}]_i$) were determined by spectrofluorometry as the changes in ratios of emissions at 510 nm when the cells were excited at 340 and 380 nm; selected cell activators were added automatically using the injector system (TECAN).

Protein phosphorylation was analyzed by immunoblotting of size-fractionated cell lysates. Cells were centrifuged and resuspended in sample buffer containing 10% SDS with or without 2-mercaptoethanol (2-ME) and then sonicated (3 × 10 s), resolved by SDS-PAGE, and immunoblotted with PY-20-HRP conjugate or with protein-specific antibodies followed by the corresponding secondary antibodies: HRP-conjugated anti-mouse, anti-rat, or anti-rabbit IgG. HRP signal was detected by the ECL reagent (Amersham Biosciences) and quantified by Luminescent Image Analyzer LAS 3000 (Fuji Photo Film Co.). Aida software (Raytest GmbH) was used for analysis.

For immunoprecipitation, postnuclear supernatants were prepared from 10–50 × 10^6 cells lysed in ice-cold lysis buffer (40) supplemented with 1% Nonidet P-40 and 1% *n*-dodecyl-β-D-maltoside (for LAT and NTAL immunoprecipitation), 1% CHAPS (for CD9 immunoprecipitation), or 0.2% Triton X-100 (for FcεRI immunoprecipitation). Target proteins were immunoprecipitated with appropriate antibodies attached to protein A/G PLUS-agarose (Santa Cruz) or Protein A UltraLink Resin (ThermoScientific).

Flow Cytometry Analysis—To quantify surface expression of CD9, BMMCs (3 × 10^5/ml) were exposed for 30 min on ice to 1–10 μg/ml of anti-CD9 followed by a 30-min incubation with FITC-conjugated anti-rat antibody. For detection of other membrane proteins, the cells were directly labeled with anti-mouse FcεRI-FITC, anti-mouse CD117-APC, or anti-mouse integrin β1-FITC conjugate. After a 30-min incubation on ice the cells were washed in ice-cold PBS and evaluated with LSRII flow cytometer (BD Biosciences). Median fluorescence intensities were determined in the FITC or APC channel and further processed using FlowJo software (Ashland, OR). For inhibition experiments, cells were pretreated with anti-CD9 mAb (10 μg/ml) for 15 min.

Chemotactic Response—Chemotactic responses were assayed using 24-well Transwell chambers (Corning) with 8-μm polycarbonate filters in the upper wells. Chemoattractants were added to the lower wells in 0.6 ml of chemotactic medium (RPMI 1640 supplemented with 1% BSA and 20 mM HEPES, pH 7.4). BMMCs (0.3 × 10^6 cells in 120 μl of chemotactic media) were added into each upper well. In experiments with Ag-mediated chemotaxis the cells were sensitized with IgE before the assay. Cells migrating into lower wells within the 8-h incubation period (37 °C, 5% CO_2 in air) were counted using Accuri C6 Flow Cytometer (BD Biosciences).

Electron Microscopy of Immunogold-labeled Membrane Sheets—Ultraclean glass coverslips (15 mm in diameter) were prepared as previously described (11). The coverslips in 24-well plates were coated by overnight incubation at 4 °C with fibronectin (50 μg/ml in PBS), followed by washing with distilled water, and used immediately. BMMCs (1.5 × 10^6) were washed twice with BSSA and then incubated on fibronectin-coated glass coverslips. After 1 h the cells were washed with BSSA and incubated with anti-CD9 antibody (15 μg/ml) in BSSA at room temperature. After 10 min the cells were washed 3 times in PBS and subsequently incubated with the secondary antibody conjugated with 12-nm gold particles. Alternatively, the cells were prefixed in 2% paraformaldehyde for 7 min, washed 3 times in PBS, and immersed in ice-cold HEPES buffer (25 mM HEPES, pH 7.0, 25 mM KCl, 2.5 mM magnesium acetate). Plasma membrane sheets were isolated and fixed in 2% paraformaldehyde in HEPES buffer for 10 min. After fixation, electron microscopy grids were transferred to PBS and target epitopes located on the cytoplasmic side of the plasma membrane were labeled with specific primary antibodies in 0.1% BSA in PBS (rabbit anti-NTAL, 1:200; rabbit anti-LAT, 1:200; mouse anti-FcεRI-β subunit mAb, clone JKR, 4 μg/ml) washed 4 times and subsequently labeled with goat anti-rabbit or anti-mouse secondary antibodies conjugated to gold nanoparticles. After extensive washing the membrane sheets were fixed in 2.5% glutaraldehyde in PBS for 10 min and the grids were transferred to PBS. After 10 min the membranes were stained with 1% OsO_4 in PBS, washed three times for 5 min in water, incubated for 10 min with 1% aqueous tannic acid, washed again in water, and stained for 10 min with 1% aqueous uranyl acetate. Finally, samples were washed twice with water for 5 min, air-dried, and observed with FEI Morgagni 268 electron microscope (FEI Czech Republic) operating at 80 kV. Typically, 10 micrographs covering 22.2 μm^2 of the cell surface were obtained from each grid; at least three independent experiments were made for each condition tested. The coordinates of gold particles were determined by ImageJ (National Institutes of Health). Statistical evaluation of colocalization of two types of particles was based on the program Gold using pair cross-correlation function (PCCF) (41).

Cell Adhesion and Spreading—IgE-sensitized BMMCs were loaded with Calcein-AM and incubated or not with anti-CD9 mAb (10 μg/ml) and/or anti-β1 integrin antibody (20 μg/ml) for 15 min before their transfer into fibronectin-coated wells. Cell adhesion was determined after a 30-min activation of the cells with Ag (50 ng/ml of TNP-BSA) using a TECAN fluorometer with excitation at 485 nm and emission at 538 nm. For cell spreading, wells of 96-well glass-bottom plates (InVitroSci) were coated with 50 μl of fibronectin in PBS (50 μg/ml). After 1 h at 22 °C the wells were washed with PBS, and 30 × 10^3 cells in BSSA were added into each well. Cells were allowed to attach for 30 min at 37 °C, gently washed, and then activated or not with Ag. After 20 min the cells were fixed for 30 min at room temperature with 3% paraformaldehyde in PBS. For filamentous (F)-actin staining, the cells were washed with 50 mM gly-

cine in PBS and then exposed to Alexa Fluor 488-phalloidin conjugate diluted 1:100 in PBS supplemented with L-α-lysophosphatidylcholine (120 μg/ml). After 1 h, the cells were washed in PBS, fixed, and kept in PBS supplemented with Hoechst 33258 stain. They were then examined with the Olympus Scan® system. Image processing and analysis were completed by means of CellProfiler software (Broad Institute, Boston, MA) (42).

Statistical Analysis—Unless specified otherwise, the significance of intergroup differences was evaluated by Student's *t* test.

RESULTS

Aggregation of CD9 Causes Activation of Mast Cells and Tyrosine Phosphorylation of NTAL but Not LAT—In an attempt to contribute to elucidating the role of membrane glycoproteins in mast cell signaling and chemotaxis we studied the properties of a new mAb prepared after immunization of a rat with cellular ghosts obtained after permeabilization of BMMCs with saponin. Previously we (30, 35, 40) and others (43, 44) showed that such ghosts are deprived of soluble cytoplasmic proteins, but possess plasma membrane proteins, cytoskeletal proteins, and nucleus. One of the mAbs prepared against such ghosts, the 2H9, was found to bind to the plasma membrane target (see below) and activate mast cells in a manner different from that known for other mast cell activators, the SCF and IgE-Ag complexes. When BMMCs were exposed to the 2H9 mAb, an increased degranulation (Fig. 1*A*) and calcium response (Fig. 1*B*) were noticed. The responses were comparable with those induced by SCF and lower than those observed in cells activated by Ag. The 2H9 mAb-induced tyrosine phosphorylation of several protein substrates in whole cell lysates was determined by immunoblotting with PY-20-HRP conjugate (Fig. 1*C*). The phosphorylation profile was, however, different from that induced by SCF or Ag (Fig. 1*C*). To identify the proteins that are phosphorylated in cells activated by 2H9 we analyzed several signaling targets using phosphospecific antibodies. For comparison we also quantified the extent of phosphorylation in cells activated by SCF and Ag. Data presented in Fig. 1*D* show that binding of 2H9 mAb had no effect on phosphorylation of Akt on Thr^{308} or Ser^{473}, and induced a weak phosphorylation of ERK and p38. Tyrosine phosphorylation profile of the whole cell lysate (Fig. 1*C*) suggested that NTAL (25–30 kDa) and LAT (36–38 kDa) could be among the proteins phosphorylated in 2H9-activated cells. To verify this, NTAL and LAT were immunoprecipitated from nonactivated or activated cells and tyrosine phosphorylation was determined using PY-20-HRP conjugate. Data in Fig. 1*E* show that tyrosine phosphorylation of NTAL in 2H9-activated cells was more pronounced than in SCF-activated cells but weaker than in Ag-activated cells. Similar analysis of LAT immunoprecipitates showed that 2H9 triggering caused only a weak LAT phosphorylation, comparable with that observed in SCF-activated cells. This was in sharp contrast to Ag-induced activation, which induced a strong phosphorylation of LAT.

Next, we attempted to identify which kinases are involved in NTAL phosphorylation in 2H9-activated cells. Previous studies showed that NTAL in Ag-activated mast cells is phosphory-

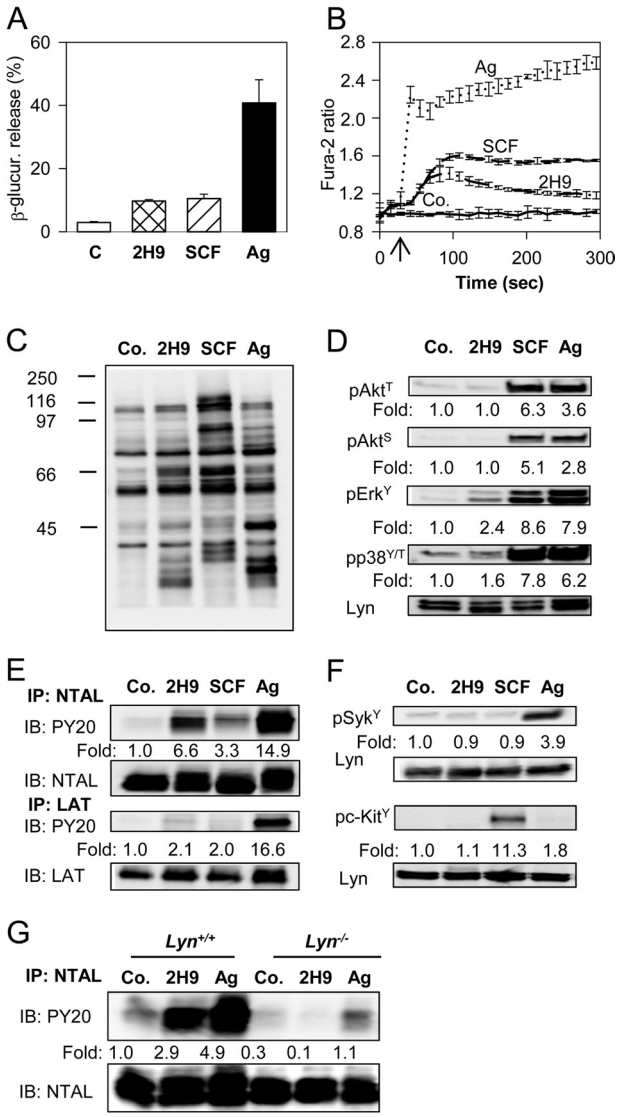

FIGURE 1. **Activation events in mast cells caused by 2H9 mAb.** BMMCs derived from WT C57BL.6 mice were sensitized overnight with TNP-specific IgE. *A,* the cells were exposed to BSSA (nonactivated control, *C*) or activated with 2H9 mAb (10 μg/ml), SCF (100 ng/ml), or Ag (500 ng/ml TNP-BSA) for 30 min. β-Glucuronidase released into supernatant was determined as described under "Experimental Procedures." Mean ± S.D. were calculated from 3 independent experiments performed in triplicates. *B,* IgE-sensitized BMMCs were loaded with Fura-2AM and exposed (*arrow*) to BSSA (*Co.*), 2H9 mAb (10 μg/ml), SCF (100 ng/ml), or Ag (500 ng/ml of TNP-BSA). Changes in $[Ca^{2+}]_i$ were determined by spectrofluorometry as the ratio of emissions at 510 nm when the cells were excited at 340 and 380 nm. *C, D,* and *F,* IgE-sensitized BMMCs were exposed to BSSA (*Co.*) or activated for 3 min with 2H9 mAb (1 μg/ml), SCF (100 ng/ml), or Ag (100 ng/ml TNP-BSA). Whole cell lysates were fractionated by SDS-PAGE and analyzed by immunoblotting with phosphotyrosine-specific mAb PY-20-HRP conjugate (*C*), antibodies specific for the indicated phosphotyrosines, pAkt-T^{308} ($pAkt^T$), pAkt-S^{473} ($pAkt^S$), pErk-Y^{204} ($pErk^Y$), and pp38-Y^{182}/T^{180} ($pp38^{Y/T}$) (*D*), or antibodies specific for pSyk-$Y^{525/526}$ ($pSyk^Y$), or pc-Kit-$Y^{568/570}$ (pc-Kit^Y) (*F*). In *D and F*, anti-Lyn mAb (*Lyn*) was used as a loading control. *E* and *G,* IgE-sensitized BMMCs derived from C57BL.6 mice (*E*) or $Lyn^{+/+}$ or $Lyn^{-/-}$ (*G*) were nonactivated (*Co.*) or activated with 2H9 mAb, SCF (*E* only), or Ag as above. The cells were solubilized in lysis buffer containing 1% Nonidet P-40 and 1% *n*-dodecyl-β-D-maltoside and postnuclear supernatants were immunoprecipitated *(IP*) with NTAL- or LAT-specific rabbit antibodies immobilized on protein A. The immunoprecipitates were analyzed by immunoblotting (*IB*) with phosphotyrosine-specific PY-20-HRP conjugate (PY20). Protein loading was determined by LAT- or NTAL-specific mAbs. In *D-G*, fold-increase in protein phosphorylation normalized to phosphorylation in nonactivated cells and protein loading is also shown. Typical results from at least 4 experiments performed are shown.

A

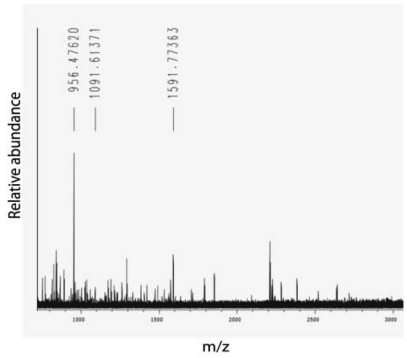

B

Identified peptides	MH+
MicroHPLC-ESI-MS/MS	
K.QLLESFQVK.P	1092.2
K.ELQEFYKDTYQK.L	1592.7
K.QLLESFQVKPC(+57)PEAISEVFNNK.F	2578.8
MALDI/FTMS	
ELQEFYK	956.4762
QLLESFQVK	1091.6137
ELQEFYKDTYQK	1591.7736

C

1 MPVKGGSKCI KYLLFGFNFI FWLAGIAVLA IGLWLRFDSQ TKSIFEQENN HSSFYTGVYI
61 LIGAGALMML VGFLGCCGAV QESQCMLGLF FGFLLVIFAI EIAAAVWGYT HKDEVIKELQ
121 EFYKDTYQKL RSKDEPQRET LKAIHMALDC CGIAGPLEQF ISDTCPKKQL LESFQVKPCP
181 EAISEVFNNK FHIIGAVGIG IAVVMIFGMI FSMILCCAIR RSREMV

D

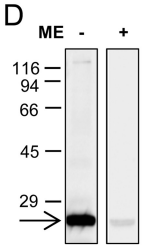

E

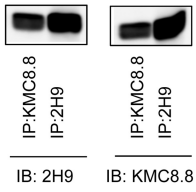

FIGURE 2. **Identification of CD9 as the target protein of 2H9 mAb.** 2H9 mAb covalently bound to protein G resin by dimethylpimelimidate was used to pulldown the target Ag from postnuclear supernatant of BMMCs lysed in a lysis buffer containing 1% Triton X-100. Bound material was eluted from the resin by SDS-PAGE sample buffer, size-fractionated on 12% SDS-PAGE, and stained with Coomassie Brilliant Blue. The major band was excised and analyzed with HPLC in combination with electrospray ionization tandem mass spectrometry (*microHPLC-ESI-MS/MS*) and MALDI-Fourier transform mass spectrometry (*MALDI/FTMS*). *A*, the chart represents the spectrum of detected peptides from trypsin-digested immunoprecipitated protein. Masses of identified peptides (*MH+*) and their corresponding peaks are indicated. *B*, table shows sequences identified by MS analysis with mass of their appropriate MH^+ ions. *C*, positions of the identified sequences (*underlined*) in the whole CD9 protein (NCBI Reference Sequence NP_031683.1). *D*, lysates from BMMCs were diluted with SDS-PAGE sample buffer supplemented with (+) or without (−) 2-mercaptoethanol (*ME*), size fractionated by SDS-PAGE, and analyzed by immunoblotting with 2H9 mAb followed by anti-rat IgG HRP conjugate. The *arrow* indicates the migration of the 2H9 target protein and *numbers on the left* represent the position of the molecular mass markers in kDa. *E*, BMMCs were lysed as in *A* and postnuclear supernatants were immunoprecipitated (*IP*) with 2H9 or KMC8.8 antibodies immobilized to protein G resin. Material released from the resin was fractionated on a 12% SDS-PAGE gel and analyzed by immunoblotting (*IB*) with 2H9 or KMC8.8 Abs. The data presented in *D* and *E* are typical results from at least 3 experiments performed.

lated by the Src family kinase Lyn, Syk kinase, and/or by KIT (45). Proper kinase activity of Syk and KIT is associated with their increased tyrosine phosphorylation (46, 47); we therefore first analyzed changes in phosphorylation of Syk and KIT. We found that these two kinases do not exhibit enhanced phosphorylation after 2H9 treatment (Fig. 1*F*). Control experiments showed, as expected, that Syk and KIT were phosphorylated in cells activated by Ag or SCF, respectively. To determine whether Lyn kinase is involved in 2H9-induced NTAL phosphorylation, NTAL was immunoprecipitated from BMMCs derived from $Lyn^{-/-}$ mice or WT ($Lyn^{+/+}$) mice. Data in Fig. 1*G* show that the absence of Lyn caused no increase in NTAL phosphorylation in 2H9-treated cells. The data suggest that Lyn is the kinase required for phosphorylation of NTAL after exposure of the cells to 2H9 mAb.

To identify the target recognized by the 2H9 mAb, we immunoprecipitated the target Ag from the lysate of resting BMMCs. The isolated material was digested with trypsin and analyzed by peptide mass mapping and peptide sequencing. Both analyses showed that 2H9 mAb binds to mouse CD9 (Fig. 2, *A-C*). The identity of the target was confirmed by decreased binding of the antibody to the cells with decreased expression of CD9 (see below). Furthermore, as determined by immunoblotting experiments, 2H9 mAb recognized a protein with a molecular mass of 22 kDa, corresponding to CD9; only unreduced samples were reactive (Fig. 2*D*). Finally, CD9 immunoprecipitated with commercially available CD9-specific antibody (KMC8.8) reacted by immunoblotting with 2H9 and vice versa (Fig. 2*E*). The combined data indicate that binding of anti-CD9 2H9 mAb induces mast cell signaling events that are different from those induced by Ag or SCF.

CD9 Colocalizes with NTAL—Previous studies showed that despite their similarity in structure and resistance to solubilization in nonionic detergents, NTAL and LAT occupy different membrane microdomains (5, 11). Tetraspanins are known to be present in both raft and nonraft regions of the plasma membrane and therefore it was of interest to determine whether CD9 colocalizes with NTAL and/or LAT. For co-localization experiments we used plasma membrane sheets isolated from BMMCs and probed them with immunogold labeling on the cytoplasmic (NTAL and LAT) or extracellular (CD9) side. Plasma membrane sheets isolated from BMMCs were fixed (i) before anti-CD9 (2H9) mAb exposure, (ii) 5 min after incubation with 2H9 mAb at 37 °C to induced CD9 dimerization, or (iii) after extensive aggregation of CD9–2H9 complexes with secondary anti-rat antibody (Fig. 3). As inferred from representative figures and PCCF analysis, NTAL exhibited some colocalization with CD9 in membranes obtained from cells

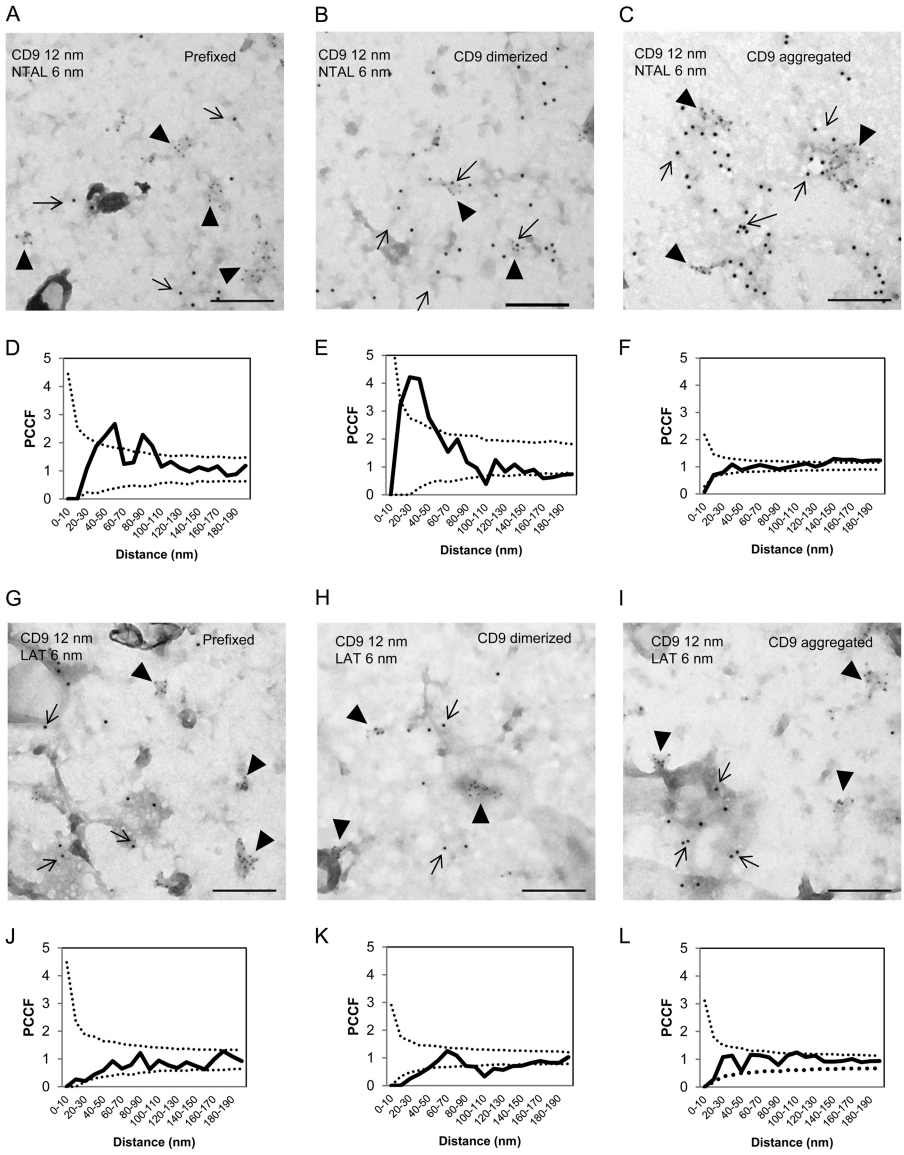

FIGURE 3. **Different colocalization of CD9 with NTAL or LAT.** BMMCs were prefixed in 2% paraformaldehyde and then stained with 2H9 mAb followed by secondary antibody conjugated to 12 nm of gold (*A, D, G,* and *J*). Alternatively, the cells were first treated with 2H9 mAb and then fixed and stained (*B, E, H,* and *K*) or the cells were first treated with 2H9 mAb followed by its aggregation with secondary antibody followed by fixation (*C, F, I,* and *L*). Plasma membrane sheets were then isolated and NTAL (*A-F*) or LAT (*G-L*) on the cytoplasmic side of the plasma membrane were labeled with primary antibodies followed by secondary antibodies conjugated to 6-nm gold particles. Topography of gold particles was evaluated by electron microscopy. Representatives from 3 independent experiments performed are shown (*A-C* and *G-I*). Evaluation of colocalization of 6- and 12-nm gold particles is represented as PCCF analysis for CD9/NTAL labeling (*D-F*) and CD9/LAT labeling (*J-L*). For calculation of PCCF, 20 μm^2 of the plasma membrane sheets was used in each experiment. PCCF indicates colocalization when experimental values (*solid line*) are higher than random distribution of particles presented by a *dotted line*. *Bars*, 200 nm.

fixed before labeling (Fig. 3, *A* and *D*). Antibody-mediated dimerization of CD9 before fixation promoted this colocalization (Fig. 3, *B* and *E*) and extensive CD9 aggregation with secondary antibody led to localization of both CD9 and NTAL in large separated clusters (Fig. 3, *C* and *F*). In contrast, LAT showed no significant colocalization with CD9 at any condition tested (Fig. 3, *G-L*). These data suggest that NTAL (unlike LAT) is located together with CD9 in membrane microdomains; this could form a mechanistical basis for their functional cross-talk.

Inhibitory Effect of Anti-CD9 on Ag-mediated Chemotaxis—Previous studies showed that tetraspanins are involved in regulation of chemotaxis in several cell types, including mast cells (48, 49). In further experiments we therefore tested the effect of the 2H9 anti-CD9 mAb on chemotaxis driven by Ag. We found that pretreatment of IgE-sensitized BMMCs with anti-CD9 mAb inhibited migration toward Ag even at low concentrations of the mAb (Fig. 4*A*). Visual microscopic inspection showed that exposure of the cells to all concentrations of the 2H9 mAb tested in the chemotaxis assays did not induce aggregation of BMMCs (not shown), which could be responsible to the observed inhibitory effect. When commercially available CD9-specific mAb, KMC8, was used, the binding to BMMCs was comparable with 2H9, but no inhibition of Ag-driven chemotaxis was observed (not shown). This suggests unique binding properties of 2H9 mAb. Previous studies showed that mast cells use tetraspanin CD9 as an alternate IL-16 receptor (48). Next we therefore examined whether anti-CD9 antibodies will interfere with IL-16-driven chemotaxis. Data presented in Fig.

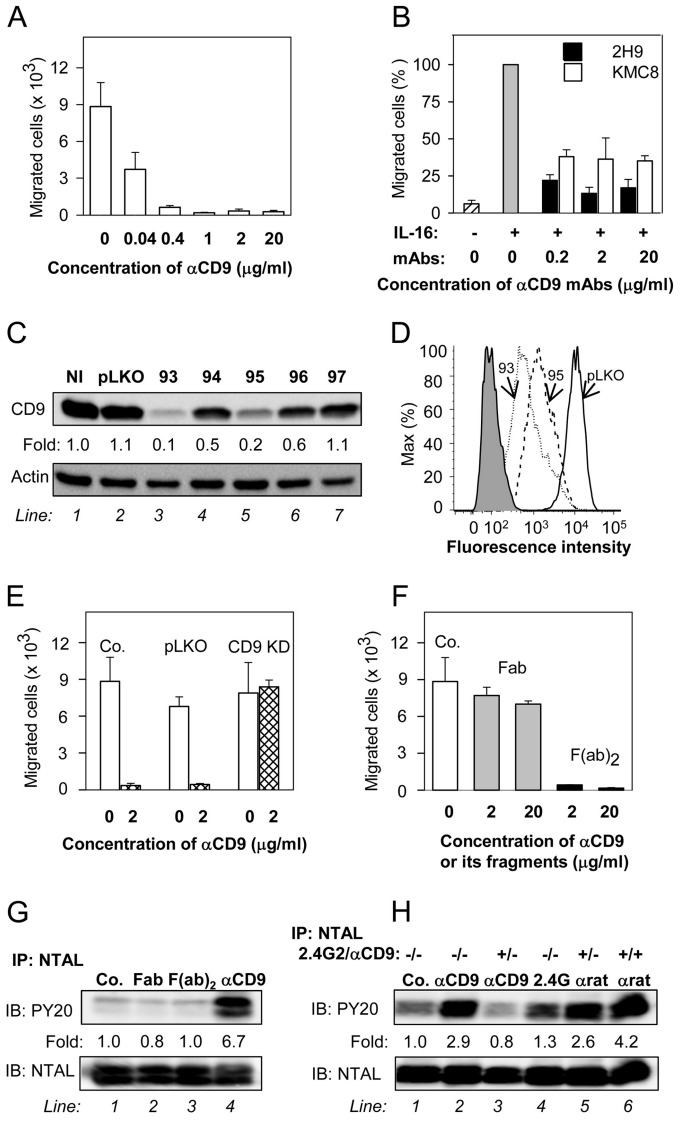

FIGURE 4. **Anti-CD9 mAb inhibits chemotaxis toward Ag and induces tyrosine phosphorylation of NTAL by different mechanism.** *A,* IgE-sensitized BMMCs were pretreated with the indicated concentrations of anti-CD9 mAb 2H9 for 15 min and their chemotactic response toward Ag (250 ng/ml of TNP-BSA in the lower chamber) was determined in the Transwell system. *B,* BMMCs were pretreated or not with the indicated concentrations of anti-CD9 antibodies (2H9 or KMC8) for 15 min and their chemotactic response toward IL-16 (50 ng/ml) was determined as above. Data were normalized toward the maximum response attained in the absence of antibody pretreatment. Migration in the absence of IL-16 is also shown. *C* and *D*, a set of murine CD9 shRNAs cloned into the pLKO.1 vector (TRCN0000066393 (*93*), TRCN0000066394 (*94*), TRCN0000066395 (*95*), TRCN0000066396 (*96*), TRCN0000066397 (*97*)) was used for lentiviral infection of BMMCs. After selection in puromycin, the cellular proteins were size fractionated by SDS-PAGE and analyzed by immunoblotting (*IB*) with anti-CD9 mAb 2H9. Actin was used as a loading control. Immunoblots were evaluated by densitometry and data were normalized to noninfected controls (*NI*) and actin amount. Similar results were obtained in at least three independent experiments. *D*, flow cytometry analysis of surface expression of CD9 in clones selected for further studies, 93 (*dotted line*) and 95 (*dashed line*). *Gray filled region* represents control cells exposed to secondary anti-rat Alexa 488 antibody alone. *Thick line* indicates cells infected with empty vector (pLKO). *E*, BMMCs were deprived of CD9 after infection with CD9 shRNA-containing vector (*CD9 KD*), uninfected cells (*Co.*), or cells infected with empty vector (*pLKO*) served as controls. Ag-mediated chemotaxis in the cells was measured as in *A*. *F*, BMMCs were not exposed (*Co.*) or exposed for 15 min to 2H9 mAb Fab or $F(ab)_2$ fragments, each at a concentration 2 or 20 μg/ml. Their chemotaxis was determined as in *A*. *G,* BMMCs were exposed to BSSA (negative control, Co., *line 1*), 2H9 mAb Fab fragment (*line 2*), 2H9 mAb $F(ab)_2$ fragment (*line 3*), or 2H9 whole molecule (αCD9; *line 4*); each at a concentration of 10 μg/ml. After 5 min the cells were solubilized in lysis buffer containing 1% Nonidet P-40 and 1% *n*-dodecyl-β-D-maltoside and postnuclear supernatants were immunoprecipitated (*IP*) with rabbit anti-NTAL antibody. The immunoprecipitates were analyzed by immunoblotting (*IB*) with phosphotyrosine-specific antibody PY-20-HRP conjugate (*PY20*) or NTAL-specific antibody as a loading control. Fold-increase in protein tyrosine phosphorylation, normalized to phosphorylation in nonactivated cells and NTAL amount is also indicated. A typical experiment from 4 performed is shown. *H,* BMMCs were pretreated or not with anti-CD16/CD32 (2.4G2; 1:50 diluted supernatant) and/or anti-CD9 mAb 2H9 (1 μg/ml, αCD9) for 15 min and then exposed to control BSSA (*Co.*, line *1*), anti-CD9 (1 μg/ml, *lines 2* and *3*), 2.4G2 antibody (1:50 diluted supernatant, *line 4*), or anti-rat IgG (1 μg/ml, *lines 5* and *6*). After 3 min the cells were lysed and NTAL was immunoprecipitated and analyzed as in *G*. Typical results from at least 3 experiments performed are shown. Mean ± S.D. in *A*, *B*, *E*, and *F* were calculated from 3 to 5 independent experiments.

4*B* indicate that both 2H9 and KMC8 inhibited chemotaxis toward IL-16; 2H9 was more potent than KMC8 at all concentrations tested.

To find out whether binding of 2H9 mAb to CD9 is indeed involved in chemotaxis inhibition, we prepared BMMCs with CD9 KD after infection of the cells with lentiviral vectors containing CD9 shRNA. From the 5 vectors used, two of them (TRCN0000066393 (*93*) and TRCN0000066395 (*95*)) strongly inhibited CD9 expression as detected by immunoblotting (Fig. 4*C*) and flow cytometry analysis (Fig. 4*D*) and were used in further experiments. Both vectors gave comparable results and therefore experimental data were pooled for presentation. Data shown in Fig. 4*E* indicate that chemotaxis toward Ag was not reduced by anti-CD9 in cells with CD9 KD, but was inhibited in control cells with empty pLKO vector. Interestingly, cells with reduced expression of CD9 showed normal migration toward Ag. These data indicate that reduced expression of CD9 is compatible with chemotaxis but not with the inhibitory effect of anti-CD9.

In macrophages (50) and platelets (51–53) anti-CD9 induced changes in signaling pathways that were caused by co-cross-linking of CD9 with FcγRs. Next we therefore studied the role of FcγRs in anti-CD9 mAb-mediated inhibition of chemotaxis. We prepared Fab and $F(ab)_2$ fragments of 2H9 mAb and compared their effects on Ag-driven chemotaxis. Pretreatment of BMMCs with anti-CD9 $F(ab)_2$ fragments had a similar inhibitory effect on chemotaxis toward Ag as caused by the whole IgG (compare Fig. 4, *A* and *F*). However, when Fab fragments were used only minimal effects were observed (Fig. 4*F*). These findings suggest that inhibition of chemotaxis is caused by aggregation of CD9 and does not require co-cross-linking of CD9 with FcγR. It should be noted that the binding capacity of the whole 2H9 IgG or its $F(ab)_2$ and Fab fragments to BMMCs was comparable as determined by flow cytometry (not shown).

CD9, Fcγ Receptors, and NTAL Phosphorylation—As shown in Fig. 1, *E* and *G*, NTAL becomes tyrosine phosphorylated after exposure of the cells to anti-CD9 mAb 2H9. The logical next step was therefore to find out whether FcγRs are involved in the process. Whereas intact 2H9 mAb induced strong tyrosine phosphorylation of NTAL (Fig. 4*G*, *line 4*), $F(ab)_2$ as well as Fab fragments of the mAb were without any effect (Fig. 4*G*, *lines 2* and *3*). In this context it should be mentioned that phosphorylation of NTAL was observed when $F(ab)_2$ or Fab fragments of the 2H9 mAb were aggregated by anti-rat IgG antibodies (not shown). These data together with the finding that 2H9 $F(ab)_2$

fragments inhibit Ag-directed chemotaxis indicate that there is no simple connection between 2H9-induced chemotaxis inhibition and NTAL tyrosine phosphorylation. It should be also mentioned that 2H9 mAb was able to induce a weak tyrosine phosphorylation of NTAL in CD9 KD cells (not shown). This indicates that aggregation of residual CD9 on cells with CD9 KD (Fig. 4*D*) is still capable to induce NTAL phosphorylation, but is no longer capable of inhibiting chemotaxis (Fig. 4*E*).

To confirm the role of Fcγ receptors in NTAL phosphorylation induced by 2H9 mAb we used rat 2.4G2 antibody, which is specific for mouse FcγRIIB/FcγRIII. BMMCs pretreated or not with a saturating concentration of 2.4G2 mAb and/or anti-CD9 mAb (1st step) was followed by exposure to anti-CD9 mAb, 2.4G2 mAb, or anti-rat IgG antibody (2nd step). The results show that the 2.4G2 antibody alone caused weak phosphorylation of NTAL (Fig. 4*H*, compare *line 1* with *line 4*). Phosphorylation of NTAL was enhanced when 2.4G2 mAb was aggregated in the 2nd step by anti-rat IgG (Fig. 4*H*, *line 5*). Pretreatment of the cells with 2.4G2 mAb followed by exposure to anti-CD9 mAb resulted in lower phosphorylation of NTAL (Fig. 4*H*, *line 3*) than after exposure of the cells to anti-CD9 alone (Fig. 4*H*, *line 2*). Maximum NTAL phosphorylation was observed when both FcγR and CD9 were extensively aggregated with the first and second layer of antibodies (Fig. 4*H*, *line 6*).

CD9 Aggregation Does Not Interfere with Early FcϵRI-mediated Signaling Events—Because 2H9 binding inhibited chemotaxis toward Ag, we were curious to know whether other Ag-induced signaling pathways are affected and whether CD9 colocalizes with FcϵRI. Our data show that FcϵRI exhibited colocalization with CD9 after CD9 dimerization or a more extensive aggregation (Fig. 5, *A-F*). Furthermore, we could demonstrate that Ag-induced degranulation (Fig. 5*G*), Ca^{2+} release (Fig. 5*H*), and tyrosine phosphorylation of Akt, ERK, and pp38 (Fig. 5*I*) were not affected by anti-CD9 mAb binding. We also found that phosphorylation of the FcϵRI-β subunit was not changed (Fig. 5*J*). These data thus indicate that signaling pathways leading to degranulation after FcϵRI triggering were not affected by anti-CD9. The experiments presented in Fig. 5 were performed with BMMCs from Balb/c mice, but similar results were obtained with BMMCs derived from C57BL/6 mice (not shown).

Different Roles of LAT and NTAL in Mast Cell Chemotaxis and Cross-talk with CD9—Data presented above show that anti-CD9 inhibits chemotaxis toward Ag and induces disparate phosphorylation of NTAL and LAT. Next we investigated the role of NTAL and LAT in mast cell chemotaxis and their sensitivity to the inhibitory effect of anti-CD9. For such experiments, BMMCs were obtained by growing progenitors from bone marrow of $Ntal^{-/-}$, $Lat^{-/-}$, 2KO mice, and corresponding controls. The cells were sensitized with TNP-specific IgE overnight and their migration toward Ag was investigated. Surprisingly, LAT-deficient cells ($Lat^{-/-}$) showed similar Ag-mediated chemotaxis as WT ($Lat^{+/+}$) cells (Fig. 6*A*). In accordance with our previous findings (14), BMMCs derived from $Ntal^{-/-}$ mice exhibited significantly higher migration toward Ag than the corresponding WT ($Ntal^{+/+}$) cells (Fig. 6*A*). These data confirm that NTAL is a negative regulator of Ag-driven chemotaxis. Interestingly, 2KO cells exhibited higher migration toward Ag than WT ($Ntal^{+/+}$ or $Lat^{+/+}$) cells or $Lat^{-/-}$ cells, but lower migration than $Ntal^{-/-}$ cells. This suggests that in the absence of NTAL even LAT negatively regulates chemotaxis. To verify that LAT and NTAL had the anticipated regulatory roles in Ag-induced degranulation, we also tested the release of β-glucuronidase after activation of the cells with Ag. Data shown in Fig. 6*B* indicate, as expected, decreased degranulation in $Lat^{-/-}$ and even more in 2KO cells and an enhanced response in $Ntal^{-/-}$ cells, when compared with the corresponding WT ($Ntal^{+/+}$ or $Lat^{+/+}$) controls.

To examine a functional regulatory cross-talk between NTAL and CD9 in chemotaxis, we compared the effect of anti-CD9 on Ag-driven chemotaxis of $Ntal^{-/-}$ and WT $Ntal^{+/+}$ cells. Data presented in Fig. 6*C* show that treatment with anti-CD9 mAb inhibited chemotaxis toward Ag in both $Ntal^{+/+}$ cells and $Ntal^{-/-}$ cells. However, $Ntal^{-/-}$ cells were more perceptive to the inhibitory effect of anti-CD9 than $Ntal^{+/+}$ cells.

CD9 Forms Complex with β1-Integrin but Anti-CD9 Does Not Interfere with β1-Integrin Function—The most prominent partners of tetraspanins are integrins (15–17, 20, 21). Next, we therefore investigated the effect of anti-CD9 mAb on integrin-mediated signaling pathways. Pretreatment of BMMCs with anti-CD9 mAb inhibited the binding of β1-integrin antibody to the cells (Fig. 7, *A* and *D*). The inhibitory effect was not affected by pretreatment with F-actin disrupting drugs, latrunculin B (0.4 μM, 30 min) or cytochalasin D (1 μM, 30 min; data not shown). This suggests that F-actin-dependent events, such as internalization, are not responsible for the observed inhibitory effect. On the other hand, pretreatment of the cells with anti-CD9 mAb had no effect on the binding of antibodies against FcϵRI and KIT (Fig. 7, *B-D*); these data support the concept that integrin is in close proximity to CD9. Immunoprecipitation data indicated that CD9 and β1-integrin are physically associated in complexes after solubilization of the cells in lysis buffer containing 1% CHAPS (Fig. 7*E*). To investigate the functional cross-talk between CD9 and β1-integrin, we tested the effect of anti-CD9 on Ag-induced adhesion of mast cells to fibronectin. It is remarkable that although anti-CD9 mAb blocked the binding of anti-β1 integrin antibody to the cells, no significant inhibition of anti-CD9 on adhesion to fibronectin was observed. As a control we used antibody against β1-integrin and found that it significantly inhibited adhesion of BMMCs to the fibronectin (Fig. 7*F*). We also tested the effect of anti-CD9 on Ag-induced spreading of mast cell on surfaces coated with fibronectin. Data presented in Fig. 7, *G* and *H*, indicate that binding of anti-CD9 at saturation concentrations to BMMCs had no significant effect on Ag-induced spreading of the cells to fibronectin. The combined data indicate that although CD9 forms complexes with β1-integrin, binding of anti-CD9 mAb does not interfere with the studied β1-integrin functions.

Cross-talk between CD9 and Cytoskeleton-regulatory Proteins of the ERM Family—An important feature of cell activation and chemotaxis is a rapid and extensive communication between plasma membrane components and cellular cytoskeleton. This process is regulated by conformational changes in ERM family proteins caused by transient dephosphorylation of their regulatory threonines. Although such changes have been documented in immunoreceptor-activated B cells, T cells, and

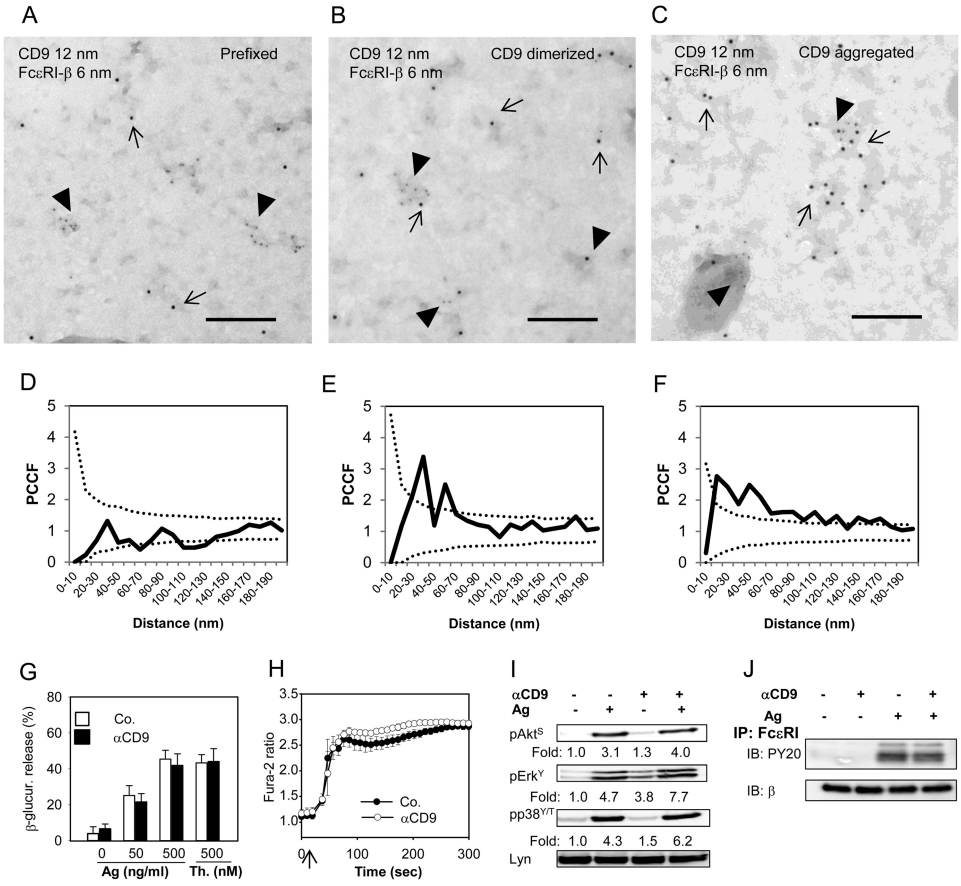

FIGURE 5. **CD9 colocalizes with FcεRI on the plasma membrane but CD9 aggregation does not interfere with early Ag-induced activation events.** *A* and *D*, BMMCs derived from Balb/c mice were prefixed with paraformaldehyde and then labeled with anti-CD9 mAb 2H9 followed by secondary anti-rat antibody-12 nm gold conjugate. Plasma membrane sheets were then isolated and the FcεRI-β subunit was labeled on the cytoplasmic side of the membrane with JRK mAb followed by secondary anti-mouse antibody-6 nm gold conjugate. Colocalization of CD9 (12 nm gold particles) and FcεRI-β (6-nm gold particles) was analyzed by electron microscopy (*A*) and evaluated by PCCF (*D*) as described in the legend to Fig. 3. *B* and *E*, BMMCs were exposed to 2H9 mAb (CD9 dimerized) before fixation and labeling for CD9; other procedures and evaluations were as in *A* and *D*. *C* and *F*, the cells were exposed to 2H9 mAb followed by the secondary anti-mouse antibody (CD9 aggregation) and then fixed and further processed as in *A* and *D*. In *A-C* representatives from 3 independent experiments are shown. *Bars*, 200 nm. *G-J*, IgE-sensitized BMMCs derived from Balb/c mice were pretreated (αCD9) or not (*Co.*; −) with anti-CD9 mAb 2H9 (10 μg/ml) for 15 min before activation. *G*, the cells were exposed to various concentrations of Ag (0–500 ng/ml TNP-BSA) or 500 nM thapsigargin (*Th.*) and 30 min later amounts of β-glucuronidase released into the cell supernatants were determined. Mean ± S.D. were calculated from at least 3 independent experiments performed in triplicates. *H*, the cells were loaded with Fura-2AM at the time of exposure to anti-CD9 and stimulated (*arrow*) with Ag (500 ng/ml of TNP-BSA). $[Ca^{2+}]_i$ was measured as described in the legend to Fig. 1*B*. Mean ± S.D. were calculated from 3 independent experiments performed in triplicates. *I*, IgE-sensitized BMMCs were exposed (+) or not (−) to anti-CD9 mAb 2H9 and then activated (+) or not (−) with Ag (100 ng/ml of TNP-BSA) for 3 min. Whole cell lysates were prepared and analyzed by immunoblotting with antibodies specific for pAkt-S^{473} (pAkt^S), pErk-Y^{204} (pErk^Y) or pp38-Y^{182}/T^{180} (pp38$^{Y/T}$); anti-Lyn mAb (*Lyn*) was used as a loading control. Fold-increase in protein phosphorylation, normalized to phosphorylation in nonactivated cells and protein loading is also shown. Typical results from at least 4 experiments performed are shown. *J*, IgE-sensitized BMMCs were exposed (+) or not (−) to anti-CD9 mAb and then activated by Ag (+; 250 ng/ml of TNP-BSA) or not (−). After 5 min the cells (15×10^6 per sample) were solubilized in lysis buffer containing 0.2% Triton X-100 and FcεRI was immunoprecipitated from postnuclear supernatants by anti-IgE antibody immobilized to Protein A beads. Tyrosine phosphorylation of the receptor subunits was evaluated with PY-20-HRP conjugate (PY-20). The amount of immunoprecipitated receptor was estimated by immunoblotting (after stripping of the membrane) with JRK mAb recognizing FcεRI β subunit. A typical experiment from 3 performed is shown.

mast cells (54–58), whether aggregation of CD9 could also induce such dephosphorylations is unknown. We have examined the phosphorylation status of the regulatory threonine after exposure of BMMCs to anti-CD9 mAb 2H9, SCF, or Ag and found that all 3 activators significantly reduced phosphorylation of the regulatory threonine (Fig. 7, *I* and *J*).

DISCUSSION

Migration of mast cell progenitors from bone marrow to connective tissues and subsequent movement of mature mast cells to the sites of inflammation is crucial for proper functioning of innate and adaptive immunity. Mast cell migration is directed by chemoattractants, which are produced by a variety of cells localized in different target tissues, as well as by intrinsic mast cell regulators that are still poorly understood (2). This study was initiated by functional screening of mAbs prepared after immunization of rats with cellular ghosts obtained by treatment of BMMCs with saponin. One of the antibodies, 2H9, recognizing tetraspanin CD9, was found capable to induce cell activation and inhibit Ag-driven mast cell chemotaxis. Several lines of evidence presented in this study indicate that 2H9-mediated CD9 aggregation triggers signaling pathways, which are different from those activated through FcεRI or KIT, and have impact on mast cell chemotaxis.

First, exposure of BMMCs to CD9-specific mAb 2H9 resulted in phosphorylation of several signal transduction proteins. Importantly, the phosphorylation profile of the target proteins differed from that produced by SCF- or Ag-mediated

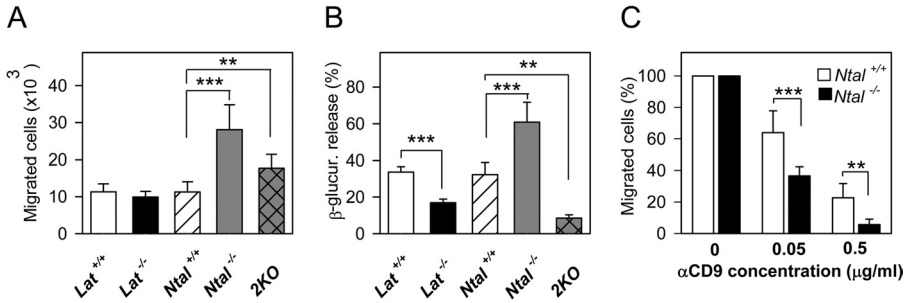

FIGURE 6. **Different roles of LAT and NTAL in mast cell chemotaxis and cross-talk with CD9.** *A*, BMMCs derived from $Lat^{-/-}$, $Ntal^{-/-}$, 2KO, and corresponding littermate ($Lat^{+/+}$, $Ntal^{+/+}$) control mice were sensitized overnight with TNP-specific IgE and their migration toward Ag (250 ng/ml of TNP-BSA) was tested in the Transwell system. *B*, the same IgE-sensitized BMMCs as in *A* were activated with Ag (250 ng/ml TNP-BSA) for 30 min and β-glucuronidase released into the supernatant was determined as described under "Experimental Procedures." *C*, BMMCs from $Ntal^{+/+}$ and $Ntal^{-/-}$ mice were sensitized with IgE and treated with the indicated concentrations of anti-CD9 mAb 2H9. Chemotaxis toward Ag was determined as in *A*. Numbers of cells migrating toward Ag were normalized to controls, 2H9 nontreated cells. Mean ± S.D. were calculated from 3 to 5 independent experiments performed in duplicates. **, $p < 0.01$; ***, $p < 0.001$.

activation (Table 1). Specifically, 2H9 mAb induced stronger phosphorylation of NTAL than activation through KIT but weaker than activation via FcεRI. On the other hand, several proteins, which were phosphorylated in KIT- and FcεRI-activated cells, were either not at all or only weakly phosphorylated after CD9 triggering (Akt, Erk, and p38). Other proteins, which were strongly phosphorylated after Ag-induced activation (Syk and LAT), showed no or only weak tyrosine phosphorylation after CD9 triggering. Enhanced phosphorylation of NTAL in anti-CD9-treated cells was only observed when whole IgG was used; Fab and $F(ab)_2$ fragments had no effect. This suggested that co-cross-linking of CD9 and Fcγ receptor(s) is required for tyrosine phosphorylation of NTAL and other targets. This conclusion was corroborated by experiments where antibody specific for FcγRIIB/FcγRIII induced tyrosine phosphorylation of NTAL, on the one hand, and, on the other, partially inhibited NTAL phosphorylation after exposure to anti-CD9. Involvement of Fcγ receptors in CD9 signaling was also described in CD9-dependent activation of platelets (53, 59) and macrophages (50).

Second, binding of anti-CD9 to target structures on the surface of mast cells resulted in weak calcium and degranulation responses, comparable with those observed in SCF-activated cells (Table 1). However, because tyrosine phosphorylation of LAT was lower in cells activated through CD9 than through KIT and because phosphorylated NTAL is unable to bind phospholipase γ and thus substitute for phosphorylated LAT in calcium metabolism (5, 6), it is evident that activation through CD9 or KIT is initiated by different activation pathways. In this connection it should be noted that pretreatment with anti-CD9 had no significant effect on subsequent binding of IgE to FcεRI and on Ag-induced degranulation, Ca^{2+} responses, and tyrosine phosphorylation of numerous substrates. In this respect, CD9 seems to differ from CD81, another tetraspanin, whose Ab-mediated aggregation inhibited Ag-induced degranulation in rat basophilic leukemia cells without affecting the Ca^{2+} response or protein tyrosine phosphorylation (60).

Third, electron microscopy studies on isolated plasma membrane sheets disclosed colocalization of CD9 with NTAL, but not with LAT, in quiescent cells. After CD9 dimerization the colocalization of CD9 with NTAL became even more prominent. This finding and the potent phosphorylation of NTAL after CD9 triggering suggest that these two molecules are physically and functionally coupled. This could explain our previous findings that although NTAL and LAT are very similar TRAPs, they, nevertheless, occupy different membrane domains (5). CD9 also colocalized with FcεRI. However, this colocalization was clearly seen only after Ab-mediated dimerization or extensive aggregation of CD9.

Fourth, pretreatment of BMMCs with anti-CD9 mAb abolished chemotaxis toward Ag. The inhibitory effect was observed not only with intact mAb but also with the corresponding $F(ab)_2$ fragment. These data suggest that the inhibitory effect is caused by CD9 aggregation and is not dependent on signals derived from cross-linking of CD9 with FcγR. This conclusion is further supported by findings that chemotaxis was not affected by Fab fragments of the anti-CD9 mAb. When another CD9-specific mAb, KMC8, was tested, no inhibition of chemotaxis was observed. This finding could be related to different epitopes recognized by 2H9 and KMC8 antibodies and/or other differences between the antibodies, such as configurational constraints (61). On the other hand, both antibodies inhibited IL-16-mediated chemotaxis by a mechanism, which seems to involve blocking binding of IL-16 to its alternate receptor, CD9 (48). We have also noticed that chemotaxis toward Ag was not affected in BMMCs with CD9 KD. This suggests that CD9 is dispensable for Ag-driven chemotaxis or that the remaining CD9 is sufficient for signal processing. Alternatively, it is possible that antibody-mediated aggregation of CD9 and CD9-bound proteins leads to uncoupling of key elements important for chemotaxis (see below).

The molecular mechanism of the inhibitory effect of anti-CD9 on Ag-induced chemotaxis seems to be complex and involves TRAPs. We found that anti-CD9 mAb was more potent in inhibiting Ag-induced chemotaxis in NTAL-deficient cells than in WT cells. This could be related to the multiple regulatory roles of NTAL and its cross-talk with CD9 and LAT (Fig. 8).

Fifth, extensive communication between plasma membrane components and the cellular cytoskeleton is crucial for immunoreceptor activation and chemotaxis. This process is regulated by conformational changes in ERM family proteins reflecting the phosphorylation status of their regulatory threonine. Our finding of increased dephosphorylation of ERM pro-

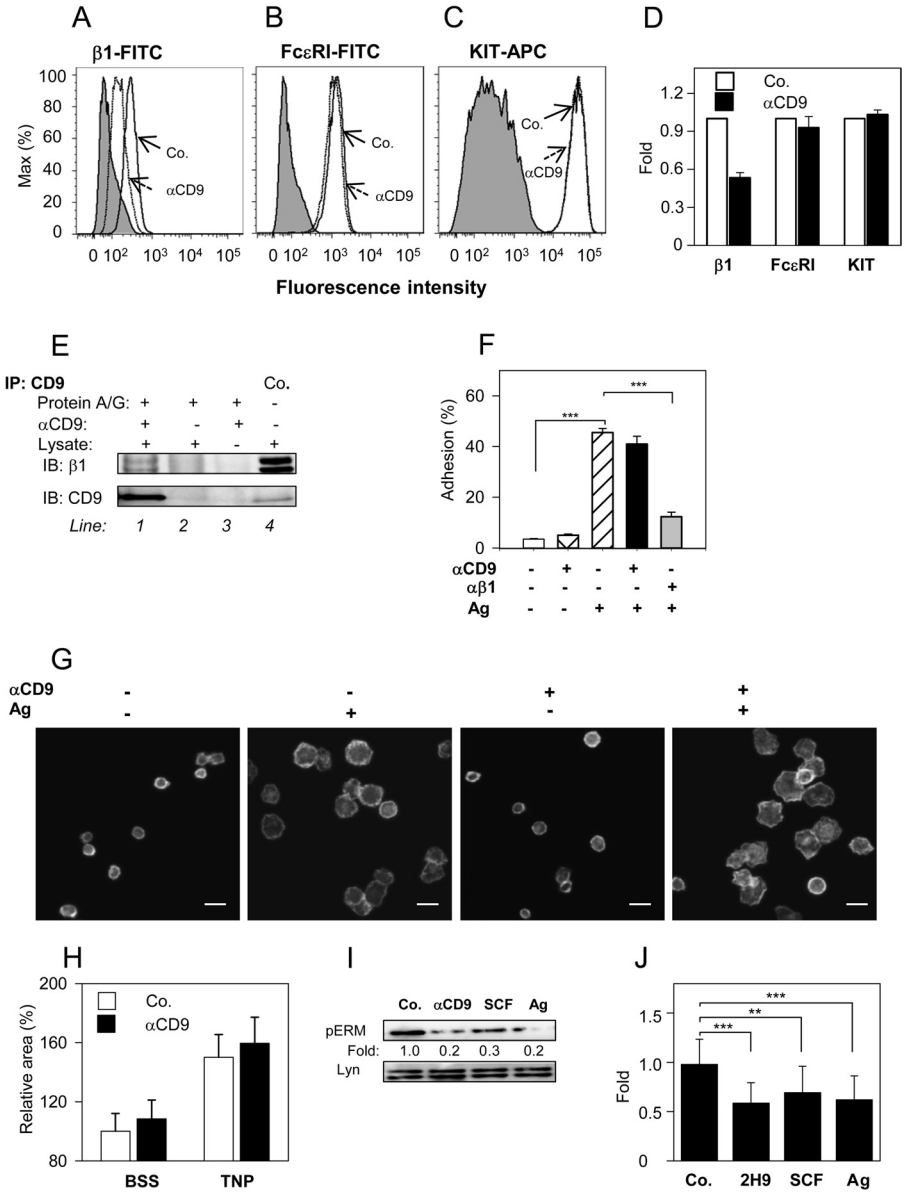

FIGURE 7. **CD9 aggregation does not interfere with β1-integrin function, but induces dephosphorylation of ERM proteins.** *A-D*, BMMCs were pretreated or not with anti-CD9 mAb 2H9 (1 μg/ml) for 15 min and the binding anti-integrin-β1-FITC conjugate (*A*), anti-FcεRI-FITC conjugate (*B*), and anti-c-Kit-APC conjugate (*C*) were estimated by flow cytometry. *Gray filled regions* represent control cells not exposed to antibodies; *dashed* and *thick lines* indicate antibody binding to anti-CD9 treated (*dashed*; αCD9) or nontreated cells (*thick*; *Co.*). *D*, data obtained as in *A-C* were normalized to maximal values obtained in the absence of anti-CD9; mean ± S.D. were determined from at least 3 independent experiments. *E*, BMMCs (10^7 per sample) were solubilized in lysis buffer supplemented with 1% CHAPS. CD9 was immunoprecipitated from postnuclear supernatants by 2H9 mAb immobilized on protein A/G beads (*line 1*). Material bound to protein A/G beads without 2H9 mAb (*line 2*) or 2H9 mAb armed protein A/G beads without cell lysate (*line 3*) served as negative controls. Whole lysates from 2.5×10^5 cells were used as positive controls (*Co.*; *line 4*). Immunoprecipitated material and controls were recovered in SDS-PAGE sample buffer with or without 2-mrecaptoethanol. Reduced and unreduced samples were immunoblotted with anti-β1 integrin (β1) or anti-CD9 (CD9), respectively. *F*, cell adhesion to fibronectin. IgE-sensitized and Calcein-loaded BMMCs were incubated with (+) or without (−) anti-CD9 mAb 2H9 and/or anti-β1 integrin antibody for 15 min before their transfer into fibronectin-coated wells. Adherence to fibronectin was determined by fluorometry after a 30-min exposure of the cells to Ag (+) or BSSA alone (−). Fluorescence was evaluated before (100%) and after washing out the non-adherent cells and percentages of adherent cells were calculated. *G*, cell spreading on fibronectin. IgE-sensitized BMMCs were pretreated (+) or not (−) with anti-CD9 mAb 2H9 and allowed to attach to fibronectin immobilized on glass surface. Then the cells were exposed (+) or not (−) to Ag for 20 min, fixed, permeabilized, and stained for actin with Alexa Fluor 488-phalloidin conjugate. Examples of the cells are shown. *Bars*, 20 μm. *H*, average areas of the cells processed as in *G* were calculated using automated CellProfiller software. Mean ± S.D. from three independent experiments, each involving ~500 cells, are shown. *I*, IgE-sensitized BMMCs were nonactivated (*Co.*) or activated with 2H9 mAb (*αCD9*), SCF, or Ag for 3 min. Whole cell lysates were prepared and analyzed by immunoblotting with *p*-ERM^T-specific Ab; anti-Lyn was used as a loading control. *Numbers* correspond to the fold-increase in phosphorylation after normalization to the total amount of protein and phosphorylation in nonactivated cells. Typical results are shown. *J*, mean ± S.D. were calculated from 10 to 18 independent experiments performed as in *I*. **, $p < 0.01$; ***, $p < 0.001$.

teins in cells exposed to anti-CD9 suggested that anti-CD9 interferes with the process of phosphorylation/dephosphorylation of ERM family members, and in this way could interfere with chemotaxis. The molecular mechanism of the cross-talk between CD9 and ERM family members is unknown. Recent studies imply an important role of the phosphorylation state of threonine in actin-binding domains of ERM proteins in cell chemotaxis (54–57). The proteins exist in an open (active) conformation with regulatory threonine phosphorylated, or closed (inactive) conformation with the regulatory threonine dephos-

TABLE 1

Comparison of anti-CD9 mAb, SCF, and Ag in their ability to induce signaling events in mast cells

Parameter[a]	Anti-CD9	SCF	Ag
Protein phosphorylation			
Akt-S^{473}	−[b]	+++	+++
Akt-T^{308}	−	+++	+++
Erk-Y^{204}	+	+++	+++
p38-T^{180}/Y^{182}	+	+++	+++
Syk	−	−	+++
NTAL	++	+	+++
LAT	−/+	−	+++
Protein dephosphorylation			
ERM-$T^{567/564/558}$	++	++	++
Degranulation (β-glucuronidase)	+	+	+++
Ca^{2+} mobilization	+	+	+++
Adhesion	−	++[c]	++
Spreading	−	+++[c]	+++
Chemotaxis	−	+++[c]	++

[a] Specific protein phosphorylation or dephosphorylation, degranulation, Ca^{2+} mobilization, adhesion, and chemotactic potential of CD9-specific mAb 2H9, SCF and Ag were measured using appropriate methods as indicated under "Experimental Procedures" and "Results."

[b] −, No signal; +, weak signal; ++, medium signal; +++, strong signal.

[c] See Ref. 14.

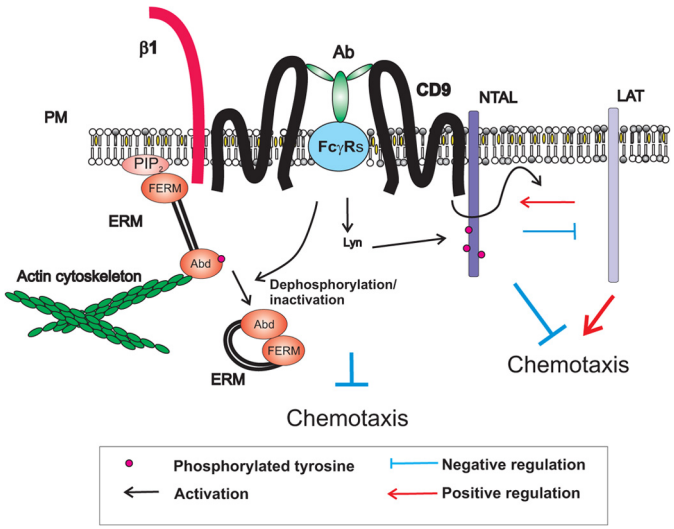

FIGURE 8. **A model of chemotaxis regulators involving CD9 and NTAL-LAT cross-talk.** Tetraspanin CD9 resides in the plasma membrane (*PM*) in close proximity to β1-integrin (β1) and NTAL. CD9-specific antibody 2H9 (*Ab*) binds to CD9 and FcγR through its Ag-binding site and Fc region, respectively. This leads to tyrosine phosphorylation of NTAL and other proteins. CD9 cross-linking also results in dephosphorylation of the regulatory threonine of ERM family proteins leading to changes in their conformation and subsequent disconnection from binding to phosphatidylinositol 4,5-bisphosphate (*PIP2*) and/or other membrane components (throughout N-terminal FERM domain) and actin cytoskeleton (through actin-binding domain, *Abd*). These and other events under certain conditions inhibit mast cell chemotaxis. Chemotaxis is also regulated by cross-talk between NTAL, LAT, and CD9. LAT and NTAL seem to be, respectively, predominantly positive and negative regulators of chemotaxis. Binding of the anti-CD9 mAb 2H9 interferes with NTAL-LAT cross-talk.

phorylated (62, 63). In the case of ezrin, the open conformation enables its binding through the actin-binding domain to F-actin and through the FERM domain to phosphatidylinositol 4,5-biphosphate on the plasma membrane, to adapter proteins or directly to cytoplasmic portions of the transmembrane molecules (59, 64). Transient dephosphorylation of the regulatory threonine disrupts this binding and has been shown to be crucial for migration of lymphocytes (54–57). A recent study with mast cells showed that dephosphorylation of the regulatory tyrosine is mediated by activity of the protein phosphatase 2A after interaction with the p21-activated kinase 1 (58). Based on our own findings and published data we propose that aggregation of CD9 leads to dephosphorylation of ERM proteins leading to their dissociation from the membrane and restrictions in communication of membrane proteins with actin cytoskeleton. This in combination with some other events involving NTAL and/or LAT contributes to inhibition of Ag-driven chemotaxis (Fig. 8). As shown in experiments with $F(ab)_2$ fragments, tyrosine phosphorylation of NTAL is not required for the inhibitory effect of anti-CD9 mAb. Nevertheless, it is possible that NTAL functions in chemotaxis even in the absence of its phosphorylation, similarly to its role in phospholipase Cγ-independent calcium uptake (12).

The combined data support the view that chemotaxis and early activation events leading to degranulation and cytokine production are processes that use different signaling pathways. The differences could be important for switching between the migratory and secretory phases depending on the concentrations of Ag and/or other chemoattractant mast cell encounters (65). At low concentrations of the Ag, mast cells migrate toward its higher concentrations. When regions of higher concentrations of the Ag are attained, the cells stop moving and activate the signaling pathways leading to secretion of the preformed allergy mediators and production and release of cytokines, leukotrienes, and other inflammatory mediators that then act as chemoattractants for other cells and/or orchestrate local immune responses. Tetraspanin CD9 and NTAL are important regulators of these events. CD9 could regulate chemotaxis through direct or indirect interactions with FcεRI, other plasma membrane receptors, and cytoskeletal components. On the other hand NTAL, which acts as a negative regulator of chemotaxis, could contribute to fine tuning of chemotaxis by competing with LAT, as suggested for its negative role in mast cell degranulation (5).

REFERENCES

1. Okayama, Y., and Kawakami, T. (2006) Development, migration, and survival of mast cells. *Immunol. Res.* **34,** 97–115
2. Halova, I., Draberova, L., and Draber, P. (2012) Mast cell chemotaxis-chemoattractants and signaling pathways. *Front Immunol.* **3,** 119
3. Wedemeyer, J., and Galli, S. J. (2000) Mast cells and basophils in acquired immunity. *Br. Med. Bull.* **56,** 936–955
4. Saitoh, S., Arudchandran, R., Manetz, T. S., Zhang, W., Sommers, C. L., Love, P. E., Rivera, J., and Samelson, L. E. (2000) LAT is essential for FcεRI-mediated mast cell activation. *Immunity* **12,** 525–535
5. Volná, P., Lebduška, P., Dráberová, L., Šímová, Š., Heneberg, P., Boubelík, M., Bugajev, V., Malissen, B., Wilson, B. S., Hořejší, V., Malissen, M., and Dráber, P. (2004) Negative regulation of mast cell signaling and function by the adaptor LAB/NTAL. *J. Exp. Med.* **200,** 1001–1013
6. Zhu, M., Liu, Y., Koonpaew, S., Granillo, O., and Zhang, W. (2004) Positive and negative regulation of FcεRI-mediated signaling by the adaptor protein LAB/NTAL. *J. Exp. Med.* **200,** 991–1000
7. Tkaczyk, C., Horejsi, V., Iwaki, S., Draber, P., Samelson, L. E., Satterthwaite, A. B., Nahm, D. H., Metcalfe, D. D., and Gilfillan, A. M. (2004) NTAL phosphorylation is a pivotal link between the signaling cascades leading to human mast cell degranulation following Kit activation and FcεRI aggregation. *Blood* **104,** 207–214
8. Draber, P., Halova, I., Levi-Schaffer, F., and Draberova, L. (2011) Transmembrane adaptor proteins in the high-affinity IgE receptor signaling. *Front. Immunol.* **2,** 95
9. Rivera, J. (2005) NTAL/LAB and LAT. A balancing act in mast-cell acti-

vation and function. *Trends Immunol.* **26,** 119–122
10. Simeoni, L., Lindquist, J. A., Smida, M., Witte, V., Arndt, B., and Schraven, B. (2008) Control of lymphocyte development and activation by negative regulatory transmembrane adapter proteins. *Immunol. Rev.* **224,** 215–228
11. Lebduška, P., Korb, J., Tůmová, M., Heneberg, P., and Dráber, P. (2007) Topography of signaling molecules as detected by electron microscopy on plasma membrane sheets isolated from non-adherent mast cells. *J. Immunol. Methods* **328,** 139–151
12. Dráberová, L., Shaik, G. M., Volná, P., Heneberg, P., Tůmová, M., Lebduska, P., Korb, J., and Dráber, P. (2007) Regulation of Ca^{2+} signaling in mast cells by tyrosine-phosphorylated and unphosphorylated non-T cell activation linker. *J. Immunol.* **179,** 5169–5180
13. Kimura, T., Hisano, M., Inoue, Y., and Adachi, M. (2001) Tyrosine phosphorylation of the linker for activator of T cells in mast cells by stimulation with the high affinity IgE receptor. *Immunol. Lett.* **75,** 123–129
14. Tůmová, M., Koffer, A., Šimíček, M., Dráberová, L., and Dráber, P. (2010) The transmembrane adaptor protein NTAL signals to mast cell cytoskeleton via the small GTPase Rho. *Eur. J. Immunol.* **40,** 3235–3245
15. Charrin, S., Le Naour, F., Oualid, M., Billard, M., Faure, G., Hanash, S. M., Boucheix, C., and Rubinstein, E. (2001) The major CD9 and CD81 molecular partner. Identification and characterization of the complexes. *J. Biol. Chem.* **276,** 14329–14337
16. Kotha, J., Longhurst, C., Appling, W., and Jennings, L. K. (2008) Tetraspanin CD9 regulates β_1 integrin activation and enhances cell motility to fibronectin via a PI-3 kinase-dependent pathway. *Exp. Cell Res.* **314,** 1811–1822
17. Levy, S., and Shoham, T. (2005) Protein-protein interactions in the tetraspanin web. *Physiology* **20,** 218–224
18. Hemler, M. E., Mannion, B. A., and Berditchevski, F. (1996) Association of TM4SF proteins with integrins. Relevance to cancer. *Biochim. Biophys. Acta* **1287,** 67–71
19. Xu, D., Sharma, C., and Hemler, M. E. (2009) Tetraspanin12 regulates ADAM10-dependent cleavage of amyloid precursor protein. *FASEB J.* **23,** 3674–3681
20. Berditchevski, F., and Odintsova, E. (1999) Characterization of integrin-tetraspanin adhesion complexes. Role of tetraspanins in integrin signaling. *J. Cell Biol.* **146,** 477–492
21. Berditchevski, F. (2001) Complexes of tetraspanins with integrins. More than meets the eye. *J. Cell Sci.* **114,** 4143–4151
22. Little, K. D., Hemler, M. E., and Stipp, C. S. (2004) Dynamic regulation of a GPCR-tetraspanin-G protein complex on intact cells: central role of CD81 in facilitating GPR56-$G\alpha_{q/11}$ association. *Mol. Biol. Cell* **15,** 2375–2387
23. Murayama, Y., Shinomura, Y., Oritani, K., Miyagawa, J., Yoshida, H., Nishida, M., Katsube, F., Shiraga, M., Miyazaki, T., Nakamoto, T., Tsutsui, S., Tamura, S., Higashiyama, S., Shimomura, I., and Hayashi, N. (2008) The tetraspanin CD9 modulates epidermal growth factor receptor signaling in cancer cells. *J. Cell Physiol.* **216,** 135–143
24. Sala-Valdés, M., Ursa, A., Charrin, S., Rubinstein, E., Hemler, M. E., Sánchez-Madrid, F., and Yáñez-Mó, M. (2006) EWI-2 and EWI-F link the tetraspanin web to the actin cytoskeleton through their direct association with ezrin-radixin-moesin proteins. *J. Biol. Chem.* **281,** 19665–19675
25. Stipp, C. S., Kolesnikova, T. V., and Hemler, M. E. (2001) EWI-2 is a major CD9 and CD81 partner and member of a novel Ig protein subfamily. *J. Biol. Chem.* **276,** 40545–40554
26. Zhang, X. A., Bontrager, A. L., and Hemler, M. E. (2001) Transmembrane-4 superfamily proteins associate with activated protein kinase C (PKC) and link PKC to specific β_1-integrins. *J. Biol. Chem.* **276,** 25005–25013
27. Hemler, M. E. (2005) Tetraspanin functions and associated microdomains. *Nat. Rev. Mol. Cell Biol.* **6,** 801–811
28. Rubinstein, E. (2011) The complexity of tetraspanins. *Biochem. Soc. Trans.* **39,** 501–505
29. Dráber, P., Zikán, J., and Vojtíšková, M. (1980) Establishment and characterization of permanent murine hybridomas secreting monoclonal anti-thy-1 antibodies. *J. Immunogenet.* **7,** 455–474
30. Smrž, D., Lebduška, P., Dráberová, L., Korb, J., and Dráber, P. (2008) Engagement of phospholipid scramblase 1 in activated cells. Implication for phosphatidylserine externalization and exocytosis. *J. Biol. Chem.* **283,** 10904–10918
31. Rudolph, A. K., Burrows, P. D., and Wabl, M. R. (1981) Thirteen hybridomas secreting hapten-specific immunoglobulin E from mice with Iga or Igb heavy chain haplotype. *Eur. J. Immunol.* **11,** 527–529
32. Rivera, J., Kinet, J. P., Kim, J., Pucillo, C., and Metzger, H. (1988) Studies with a monoclonal antibody to the β subunit of the receptor with high affinity for immunoglobulin E. *Mol. Immunol.* **25,** 647–661
33. Brdička, T., Imrich, M., Angelisová, P., Brdičková, N., Horváth, O., Špička, J., Hilgert, I., Lusková, P., Dráber, P., Novák, P., Engels, N., Wienands, J., Simeoni, L., Osterreicher, J., Aguado, E., Malissen, M., Schraven, B., and Hořejší, V. (2002) Non-T cell activation linker (NTAL). A transmembrane adaptor protein involved in immunoreceptor signaling. *J. Exp. Med.* **196,** 1617–1626
34. Tolar, P., Tůmová, M., and Dráber, P. (2001) *Folia Biol.* **47,** 215–217
35. Dráberová, L., Amoui, M., and Dráber, P. (1996) Thy-1-mediated activation of rat mast cells. The role of Thy-1 membrane microdomains. *Immunology* **87,** 141–148
36. Kovářová, M., Tolar, P., Arudchandran, R., Dráberová, L., Rivera, J., and Dráber, P. (2001) Structure-function analysis of Lyn kinase association with lipid rafts and initiation of early signaling events after Fcϵ receptor I aggregation. *Mol. Cell Biol.* **21,** 8318–8328
37. Hibbs, M. L., Tarlinton, D. M., Armes, J., Grail, D., Hodgson, G., Maglitto, R., Stacker, S. A., and Dunn, A. R. (1995) Multiple defects in the immune system of Lyn-deficient mice, culminating in autoimmune disease. *Cell* **83,** 301–311
38. Hájková, Z., Bugajev, V., Dráberová, E., Vinopal, S., Dráberová, L., Janáček, J., Dráber, P., and Dráber, P. (2011) STIM1-directed reorganization of microtubules in activated mast cells. *J. Immunol.* **186,** 913–923
39. Surviladze, Z., Dráberová, L., Kovářová, M., Boubelík, M., and Dráber, P. (2001) Differential sensitivity to acute cholesterol lowering of activation mediated via the high-affinity IgE receptor and Thy-1 glycoprotein. *Eur. J. Immunol.* **31,** 1–10
40. Hálová, I., Dráberová, L., and Dráber, P. (2002) A novel lipid raft-associated glycoprotein, TEC-21, activates rat basophilic leukemia cells independently of the type 1 Fcϵ receptor. *Int. Immunol.* **14,** 213–223
41. Philimonenko, A. A., Janáček, J., and Hozák, P. (2000) Statistical evaluation of colocalization patterns in immunogold labeling experiments. *J. Struct. Biol.* **132,** 201–210
42. Carpenter, A. E., Jones, T. R., Lamprecht, M. R., Clarke, C., Kang, I. H., Friman, O., Guertin, D. A., Chang, J. H., Lindquist, R. A., Moffat, J., Golland, P., and Sabatini, D. M. (2006) CellProfiler. Image analysis software for identifying and quantifying cell phenotypes. *Genome Biol.* **7,** R100
43. Fiskum, G., Craig, S. W., Decker, G. L., and Lehninger, A. L. (1980) The cytoskeleton of digitonin-treated rat hepatocytes. *Proc. Natl. Acad. Sci. U.S.A.* **77,** 3430–3434
44. Bangham, A. D., Horne, R. W., Glauert, A. M., Dingle, J. T., and Lucy, J. A. (1962) Action of saponin on biological cell membranes. *Nature* **196,** 952–955
45. Iwaki, S., Spicka, J., Tkaczyk, C., Jensen, B. M., Furumoto, Y., Charles, N., Kovarova, M., Rivera, J., Horejsi, V., Metcalfe, D. D., and Gilfillan, A. M. (2008) Kit- and FcϵRI-induced differential phosphorylation of the transmembrane adaptor molecule NTAL/LAB/LAT2 allows flexibility in its scaffolding function in mast cells. *Cell Signal* **20,** 195–205
46. Zhang, J., Billingsley, M. L., Kincaid, R. L., and Siraganian, R. P. (2000) Phosphorylation of Syk activation loop tyrosines is essential for Syk function. An *in vivo* study using a specific anti-Syk activation loop phosphotyrosine antibody. *J. Biol. Chem.* **275,** 35442–35447
47. Linnekin, D. (1999) Early signaling pathways activated by c-Kit in hematopoietic cells. *Int. J. Biochem. Cell Biol.* **31,** 1053–1074
48. Qi, J. C., Wang, J., Mandadi, S., Tanaka, K., Roufogalis, B. D., Madigan, M. C., Lai, K., Yan, F., Chong, B. H., Stevens, R. L., and Krilis, S. A. (2006) Human and mouse mast cells use the tetraspanin CD9 as an alternate interleukin-16 receptor. *Blood* **107,** 135–142
49. Krämer, B., Schulte, D., Körner, C., Zwank, C., Hartmann, A., Michalk, M., Söhne, J., Langhans, B., Nischalke, H. D., Coenen, M., Möhl, C., Vogt, A., Hennenberg, M., Sauerbruch, T., Spengler, U., and Nattermann, J. (2009) Regulation of NK cell trafficking by CD81. *Eur. J. Immunol.* **39,** 3447–3458

50. Kaji, K., Takeshita, S., Miyake, K., Takai, T., and Kudo, A. (2001) Functional association of CD9 with the Fcγ receptors in macrophages. *J. Immunol.* **166,** 3256–3265
51. Kuroda, K., Ozaki, Y., Qi, R., Asazuma, N., Yatomi, Y., Satoh, K., Nomura, S., Suzuki, M., and Kume, S. (1995) FcγII receptor-mediated platelet activation induced by anti-CD9 monoclonal antibody opens Ca^{2+} channels which are distinct from those associated with Ca^{2+} store depletion. *J. Immunol.* **155,** 4427–4436
52. Qi, R., Ozaki, Y., Kuroda, K., Asazuma, N., Yatomi, Y., Satoh, K., Nomura, S., and Kume, S. (1996) Differential activation of human platelets induced by Fcγ receptor II cross-linking and by anti-CD9 monoclonal antibody. *J. Immunol.* **157,** 5638–5645
53. Worthington, R. E., Carroll, R. C., and Boucheix, C. (1990) Platelet activation by CD9 monoclonal antibodies is mediated by the Fcγ II receptor. *Br. J. Haematol.* **74,** 216–222
54. Gupta, N., Wollscheid, B., Watts, J. D., Scheer, B., Aebersold, R., and DeFranco, A. L. (2006) Quantitative proteomic analysis of B cell lipid rafts reveals that ezrin regulates antigen receptor-mediated lipid raft dynamics. *Nat. Immunol.* **7,** 625–633
55. Liu, Y., Belkina, N. V., Park, C., Nambiar, R., Loughhead, S. M., Patino-Lopez, G., Ben-Aissa, K., Hao, J. J., Kruhlak, M. J., Qi, H., von Andrian, U. H., Kehrl, J. H., Tyska, M. J., and Shaw, S. (2012) Constitutively active ezrin increases membrane tension, slows migration, and impedes endothelial transmigration of lymphocytes *in vivo* in mice. *Blood* **119,** 445–453
56. Parameswaran, N., Matsui, K., and Gupta, N. (2011) Conformational switching in ezrin regulates morphological and cytoskeletal changes required for B cell chemotaxis. *J. Immunol.* **186,** 4088–4097
57. Treanor, B., Depoil, D., Bruckbauer, A., and Batista, F. D. (2011) Dynamic cortical actin remodeling by ERM proteins controls BCR microcluster organization and integrity. *J. Exp. Med.* **208,** 1055–1068
58. Staser, K., Shew, M. A., Michels, E. G., Mwanthi, M. M., Yang, F. C., Clapp, D. W., and Park, S. J. (2013) A Pak1-PP2A-ERM signaling axis mediates F-actin rearrangement and degranulation in mast cells. *Exp. Hematol.* **41,** 56–66
59. Yonemura, S., Hirao, M., Doi, Y., Takahashi, N., Kondo, T., Tsukita, S., and Tsukita, S. (1998) Ezrin/radixin/moesin (ERM) proteins bind to a positively charged amino acid cluster in the juxta-membrane cytoplasmic domain of CD44, CD43, and ICAM-2. *J. Cell Biol.* **140,** 885–895
60. Fleming, T. J., Donnadieu, E., Song, C. H., Laethem, F. V., Galli, S. J., and Kinet, J. P. (1997) Negative regulation of FcεRI-mediated degranulation by CD81. *J. Exp. Med.* **186,** 1307–1314
61. Ortega, E., Schweitzer-Stenner, R., and Pecht, I. (1988) Possible orientational constraints determine secretory signals induced by aggregation of IgE receptors on mast cells. *EMBO J.* **7,** 4101–4109
62. Gary, R., and Bretscher, A. (1995) Ezrin self-association involves binding of an N-terminal domain to a normally masked C-terminal domain that includes the F-actin binding site. *Mol. Biol. Cell* **6,** 1061–1075
63. Reczek, D., and Bretscher, A. (1998) The carboxyl-terminal region of EBP50 binds to a site in the amino-terminal domain of ezrin that is masked in the dormant molecule. *J. Biol. Chem.* **273,** 18452–18458
64. Hirao, M., Sato, N., Kondo, T., Yonemura, S., Monden, M., Sasaki, T., Takai, Y., Tsukita, S., and Tsukita, S. (1996) Regulation mechanism of ERM (ezrin/radixin/moesin) protein/plasma membrane association. Possible involvement of phosphatidylinositol turnover and Rho-dependent signaling pathway. *J. Cell Biol.* **135,** 37–51
65. Gonzalez-Espinosa, C., Odom, S., Olivera, A., Hobson, J. P., Martinez, M. E., Oliveira-Dos-Santos, A., Barra, L., Spiegel, S., Penninger, J. M., and Rivera, J. (2003) Preferential signaling and induction of allergy-promoting lymphokines upon weak stimulation of the high affinity IgE receptor on mast cells. *J. Exp. Med.* **197,** 1453–1465